Proceedings of the
Annual Stability Conference
Structural Stability Research Council
Denver, Colorado, March 22-25, 2022

Buckling behavior of open-web steel joists and joist girders

Edward J. Sippel[1], Ronald D. Ziemian[2], Hannah B. Blum[3]

Abstract

Open-web steel joists are often fabricated from components with relatively high slenderness ratios to efficiently support loading. As a result, joists are susceptible to buckling instabilities in the webs and the double angle chords. The current SJI design requirements for steel joists require the consideration of flexural buckling but exclude any consideration of flexural-torsional buckling modes for double angle members, which differs from AISC's design requirements. This study evaluates the underlying SJI assumption that flexural-torsional buckling can be neglected in joist design. This paper reports on the theoretical inelastic buckling behavior of double angles and the details of the finite element model required for accurately simulating the stability behavior. The theoretical investigation applied the methodology behind AISC's treatment of single angle flexural-torsional buckling to verify the expected response for double angles in joist and joist girder applications. The results identified several double angle geometries that appear to be susceptible to flexural-torsional buckling. Next, finite element models of the joist and joist girders are presented, which are validated by making comparisons with previously reported full steel joists experimental results including web-to-chord connection variations, support and bracing conditions, and loading application. These validation models were able to accurately predict the bending stiffness of the joist and the different buckling failure modes of the webs. The results indicated that flexural-torsional buckling is not as critical for design as indicated by AISC. This behavior was further verified using isolated chord models.

1. Introduction

Steel joist and joist girders are economical steel structures that can be used in a variety of applications. The efficient use of material often results the use of in slender elements that are susceptible to buckling under compression. The current Steel Joist Institute (SJI) Standard Specification for K-Series, LH-Series, DLH-Series Open Web Steel Joists and for Joist Girders (SJI 100-2020) (2020) requires that the design capacity of hot-rolled sections account for flexural and local buckling effects. These requirements contrast with the current provisions of the American Institute of Steel Construction (AISC) Specification for Structural Steel Buildings (2016) which additionally

[1]Graduate Research Assistant, University of Wisconsin-Madison, <esippel@wisc.edu>
[2]Professor, Bucknell University, <ziemian@bucknell.edu>
[3]Assistant Professor and Alain H. Peyrot Fellow, University of Wisconsin-Madison, <hannah.blum@wisc.edu>

require consideration of flexural-torsional buckling. For non-doubly symmetric members such as angles and double angles, flexural-torsional buckling can often lead to significantly lower design capacities at short lengths. A study on double angle buckling by Simpson Gumpertz & Heger Inc. (2011) noted that the flexural-torsional behavior required by the AISC Specification produced overly conservative results at low slenderness ratios while the SJI Specification resulted in somewhat unconservative capacities for some geometries. Since that study occurred, alterations have been made to provisions regarding local buckling reductions and modified slenderness of composite members; however, the major global buckling discrepancy between the two Specifications has not been addressed. This paper summarizes an investigation into the behavior of double angles used for joist and joist girder chords including the theoretical response and a parametric numerical study of full-scale joists and joist chord segments. The joist modeling validation is also discussed.

2. Theoretical Buckling Capacity

2.1. Background

The foundation of compression member design is elastic buckling that incorporates the global limits of flexural, torsional, or combined flexural-torsional buckling and local effects. The critical flexural buckling stress about the x-axis, f_x, and about the y-axis, f_y, are calculated by Eq. 1 and Eq. 2, respectively. Torsional buckling occurs due to twisting about the shear center with a critical torsional buckling stress, f_z, determined by Eq. 3;

$$f_x = \frac{\pi^2 E}{(L/r_x)^2} \tag{1}$$

$$f_y = \frac{\pi^2 E}{(L/r_y)^2} \tag{2}$$

$$f_z = \frac{GJ + \pi^2 E C_w / L^2}{r_0^2 A} \tag{3}$$

where E is the modulus of elasticity, G is the shear modulus, $r_x = \sqrt{I_x/A}$ and $r_y = \sqrt{I_y/A}$ are the radii of gyration about the x- and y- axes, I_x and I_y are the moments of inertia about the principal x- and the y-axes, A is the cross-sectional area, J is the torsion constant, C_w is the warping constant, L is the unbraced length, and r_0 is the polar radius of gyration about the shear center which is calculated by Eq. 4;

$$r_0^2 = r_x^2 + r_y^2 + x_0^2 + y_0^2 \tag{4}$$

where (x_0, y_0) are the coordinates of the shear center relative to the centroid.

In an arbitrary section, the flexural and torsional buckling modes can interact which introduces flexural-torsional buckling. This interaction is defined by Eq. 5 where the three roots of the equation are the critical buckling stresses, f_{el} (Trahair, 1993). When the shear center and centroid are

coincident, Eq. 5 reduces to uncoupled flexural and torsional buckling modes with the minimum value controlling the behavior. When the shear center and centroid are not coincident, such as double angle cross sections, the interaction of buckling modes results in a new lower buckling stress.

$$(f_{el} - f_x)(f_{el} - f_y)(f_{el} - f_z) - f_{el}^2 (f_{el} - f_y)\frac{x_0^2}{r_0^2} - f_{el}^2 (f_{el} - f_x)\frac{y_0^2}{r_0^2} = 0 \tag{5}$$

Slender cross section elements experience local buckling, which is incorporated into hot-rolled member design based on the plate buckling stress, f_L , given by Eq. 6;

$$f_L = \frac{0.425\pi^2 E}{12(1-\nu^2)}\left(\frac{t}{b}\right)^2 \tag{6}$$

where ν is the Poisson's ratio, t is the thickness of the angle leg, and b is the leg width. For unstiffened elements such as the legs of single and double angles, the failure mode assumes uniform one-way compression on a pin supported plate with one edge supported and the other unsupported.

Building upon the elastic buckling response, inelastic buckling design per both the SJI Specification (SJI, 2020) and the AISC Specification (AISC, 2016) utilizes a tangential buckling approach based on flexural buckling behavior to convert the limiting elastic buckling stress, F_e, to the critical buckling stress, F_{cr}. At low compressive buckling stresses, the behavior remains largely elastic and can be determined using Eq. 7. When F_e exceeds $\frac{4}{9}$ of the yield stress, F_y, inelastic buckling behavior controls and is represented by Eq. 8.

$$F_{cr} = 0.877F_e \quad \text{for } \frac{F_y}{F_e} > 2.25 \tag{7}$$

$$F_{cr} = \left(0.658^{F_y/F_e}\right)F_y \quad \text{for } \frac{F_y}{F_e} \leq 2.25 \tag{8}$$

An alternative method of presenting this relationship would be to use a reduction factor, τ, to directly calculate the tangential buckling response by modifying E (Galambos, 1991). Rearranging Eqs. 7 and 8, the F_{cr} can instead be defined as the limiting elastic buckling capacity times τ given by Eq. 9.

$$\tau = \begin{cases} 0.877 & \text{if } \frac{F_{cr}}{F_y} \leq 0.877/2.25 \\ \frac{1}{\ln(0.658)}\frac{F_{cr}}{F_y}\ln\left(\frac{F_{cr}}{F_y}\right) & \text{otherwise} \end{cases} \tag{9}$$

Lastly, a modification factor that accounts for strength reduction due to local buckling is included. The current SJI Specification and the prior AISC Specification (AISC, 2010) utilized a single slenderness reduction factor, Q, according to Eq. 10;

$$Q = \begin{cases} 1.0 & \text{if } \lambda_e \leq 0.45\sqrt{\frac{E}{F_y}} \\ 1.34 - 0.76\lambda_e\sqrt{\frac{F_y}{E}} & \text{if } 0.45\sqrt{\frac{E}{F_y}} < \lambda_e \leq 0.91\sqrt{\frac{E}{F_y}} \\ 0.53\frac{E}{F_y}\left(\frac{1}{\lambda_e}\right)^2 & \text{if } 0.91\sqrt{\frac{E}{F_y}} < \lambda_e \end{cases} \tag{10}$$

where λ_e is the slenderness of the angle leg, b/t.

For double angles, the single lowest Q factor associated with any unstiffened element is used to uniformly reduce the capacity of the entire section. This local buckling limitation is incorporated by replacing F_y in Eq. 7, 8, and 9 with QF_y and the remaining calculations are completed as normal. The 2016 AISC Specification introduced a different approach requiring the original F_{cr} to act over an effective area of the cross section based on plate buckling. While the different local buckling provisions alter the final capacities, the impact of this variation is not discussed in further detail in this paper because the focus of this study is on the current SJI requirements.

The design buckling calculations have been limited to flexural buckling since it is the foundation of compression member design. The current SJI Specification allows for the effects of flexural-torsional buckling to be neglected for double and single angles, and, as a result, only flexural buckling need be considered. The AISC Specification incorporates a similar exception for single angles, but requires the consideration of flexural-torsional buckling for double angles. The capacity is conservatively calculated by using the minimum elastic buckling response considering flexural and flexural-torsional buckling modes using Eq. 5 and applies the same flexural buckling reduction shown in Eq. 7 and 8. However, this approach does not account for the strength associated with the shear stiffness as identified in previous testing and numerical studies (Galambos, 1991; Galambos, 1963; Kitipornchai and Lee, 1986; Trahair and Kitipornchai, 1972). Unlike the softening longitudinal behavior, shear stiffness has been found to remain effectively constant until full yield of the section, which can result in higher and more realistic torsional buckling capacities. The inelastic shear and longitudinal responses can be combined by modifying Eq. 5 with the appropriate tangential stiffness reduction factor, τ for the longitudinal behavior and τ_G for the shear behavior, resulting in Eq. 11 where the minimum solution is the inelastic critical buckling stress, f_{in}. Previous work by Galambos (1991) determined that accounting for the increased stiffness meant flexural-torsional buckling was unlikely to control the design of single angles when accounting for the interaction of flexural buckling and local buckling. That study also determined that some double angles were susceptible to flexural-torsional buckling and recommended continuing to consider the relevant provisions for the design of double angles.

$$\begin{aligned} &\left(f_{in} - f_x\tau\right)\left(f_{in} - f_y\tau\right)\left(f_{in} - \frac{\tau_G GJ + \tau\pi^2 EC_w/L^2}{r_0^2}\right) \\ &-f_{in}^2\left(f_{in} - f_y\tau\right)\frac{x_0^2}{r_0^2} - f_{in}^2\left(f_{in} - f_x\tau\right)\frac{y_0^2}{r_0^2} = 0 \end{aligned} \tag{11}$$

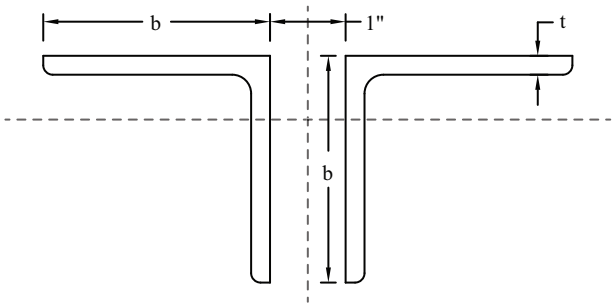

Figure 1: Typical double angle chord geometry

Table 1: Angle dimensions considered

Leg (in)	Thickness (in)								
1.25	0.109	0.115	0.125	0.188					
1.5	0.109	0.115	0.123	0.137	0.141	0.155	0.17	0.188	0.25
1.75	0.115	0.125	0.143	0.155	0.17	0.188	0.25		
2	0.125	0.143	0.156	0.163	0.176	0.188	0.205	0.216	0.23
2 (cont.)	0.248	0.25	0.281	0.313					
2.5	0.188	0.212	0.23	0.25	0.28	0.313			
3	0.188	0.227	0.25	0.281	0.29	0.313	0.375		
3.5	0.287	0.313	0.344	0.375					
4	0.25	0.313	0.344	0.375	0.438	0.5			
5	0.438	0.5							
6	0.438	0.5	0.563	0.625	0.75	0.875	1		
8	0.5	0.546	0.625	0.75	1	1.125			

2.2. Inelastic Buckling Study

Galambos's (1991) recommendation for double angles covered a wide array of geometries including both unequal- and equal-leg sections, multiple spacings between the vertical legs of the angles, and different connection methods. For this study, a more limited configuration was considered to investigate the impact of flexural-torsional behavior in joist and joist girder chords. Only equal-leg double angles spaced with one inch between the vertical legs as shown in Fig. 1 were considered. Table 1 summarizes the chord double angle dimensions evaluated for this study, which are representative of joist designs per SJI.

This flexural-torsional buckling study included variations in the shear stiffness via two values for τ_G and in the warping stiffness of double angles via three values for C_w. In line with previous research (Galambos, 1991; Kitipornchai and Lee, 1986; Neal, 1950), an upper limit of $\tau_G = 1.0$ was used to capture the full shear stiffness of the section as minimal reduction was observed. A reduction was estimated as $\tau_G = 0.877$ to account for imperfections and residual stresses based on critical elastic flexural buckling. The minimum value for C_w was defined based on AISC's (AISC, 2016) conservative design recommendation that C_w of double angles can be taken as 0 and the shear center, S_{low}, is positioned along the axis of symmetry at the middle of the horizontal flanges similar to a tee section as shown in Fig. 2. An alternative conservative recommendation by the Canadian Institute of Steel Construction (CISC, 2002) uses the same shear center position but

Figure 2: Assumed double angle warping behavior (a) AISC/CISC (b) Est. upper bound

references a C_w equal to twice that of the single angle. Limited information was available on the composite twist response of double angles; therefore, an estimate of a fully composite behavior was determined using a thin-walled approximation by assuming a connection between the angle heels with no thickness which resulted in a new shear center, S_{high}, and a significantly increased C_w, by more than a factor of 100 in some configurations. These three C_w values were considered to investigate the impact of warping stiffness and are identified as $C_w = 0$, Low C_w, and High C_w, respectively.

For each alternative C_w, four inelastic buckling curves were determined for lengths up to 200 times the minimum radius of gyration. The upper bound was determined considering flexural buckling effects in line with the current SJI Specification and labeled "FB". The lower bound for capacity was determined considering both flexural and torsional buckling effects aligned with the AISC Specification and labeled "FTB". Two intermediate solutions were found using the τ_G factors discussed above to capture the increased shear stiffness in torsional buckling. The results labeled "$\tau_G = 1.0$" account for the maximum increase in strength while the results labeled "$\tau_G = 0.877$" include a small reduction to account for imperfections. All calculations included local buckling reductions based on the SJI provisions, which employ the previously mentioned Q-factor.

The study identified multiple double angle configurations expected to be controlled by flexural buckling over flexural-torsional buckling. Compact sections, such as the 2-L8"x8"x1" shown in Fig. 3, were controlled by flexural buckling about the x-axis once accounting for the increased shear stiffness. However, this trend was not absolute and flexural-torsional buckling became the controlling mechanism as the legs became more slender as depicted in Fig. 4 and Fig. 5. Accounting for a non-zero C_w significantly increased the capacity in flexural-torsional buckling, especially when considering a composite response. Despite the increases indicated, multiple double angle cross sections were still controlled by flexural-torsional buckling with significantly lower capacities. This result does not align with the well-established history of existing joist performance and various production testing that indicate joists and joist girders are adequately designed by only considering flexural buckling. As a consequence, further investigation using advanced finite element models was implemented to validate the theoretical results by evaluating systems where flexural-torsional buckling was expected to control the response.

3. Joist finite element modeling validation

The joist finite element modeling procedure was validated using previous work by Yost et al. (2004; 2006) that tested a series of 16-foot (4.88 m) long, 18 inch (460 mm) and 30 inch (760 mm) deep steel joists until failure via web member buckling. The joists were constructed with 2-L2"x2"x0.125" double angle chords, crimped end L1"x1"x0.125" angle webs, and an end 7/8-

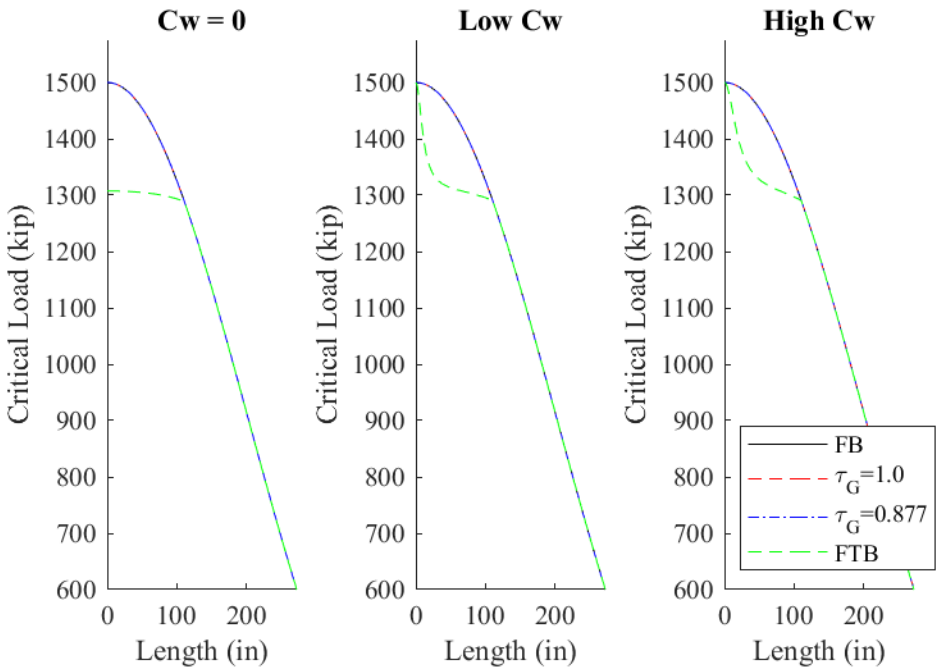

Figure 3: Inelastic buckling of a 2-L8”x8”x1” controlled by flexural buckling

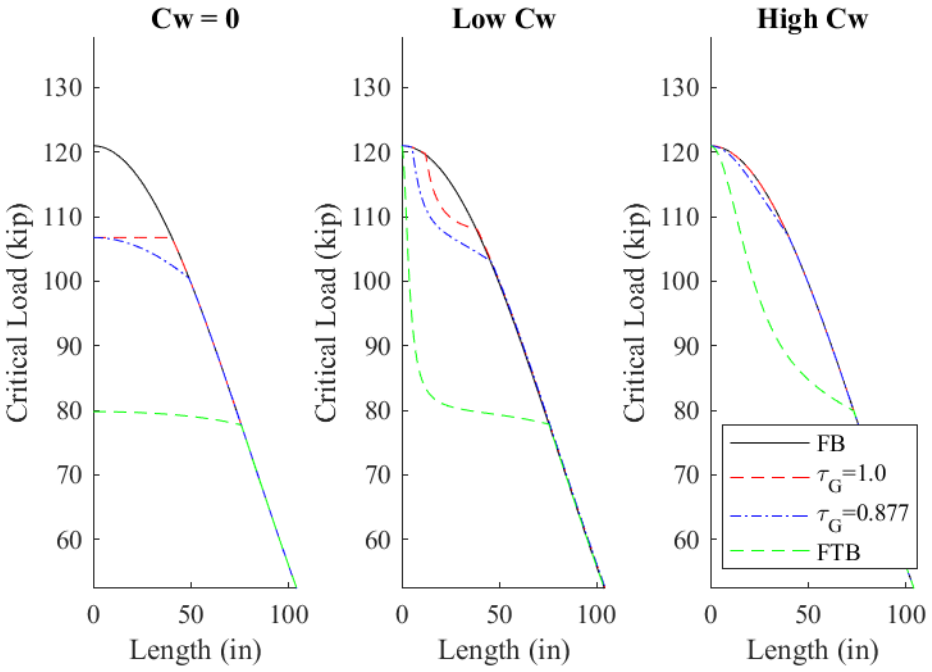

Figure 4: Inelastic buckling of a 2-L3”x3”x0.227” with limited critical flexural-torsional buckling

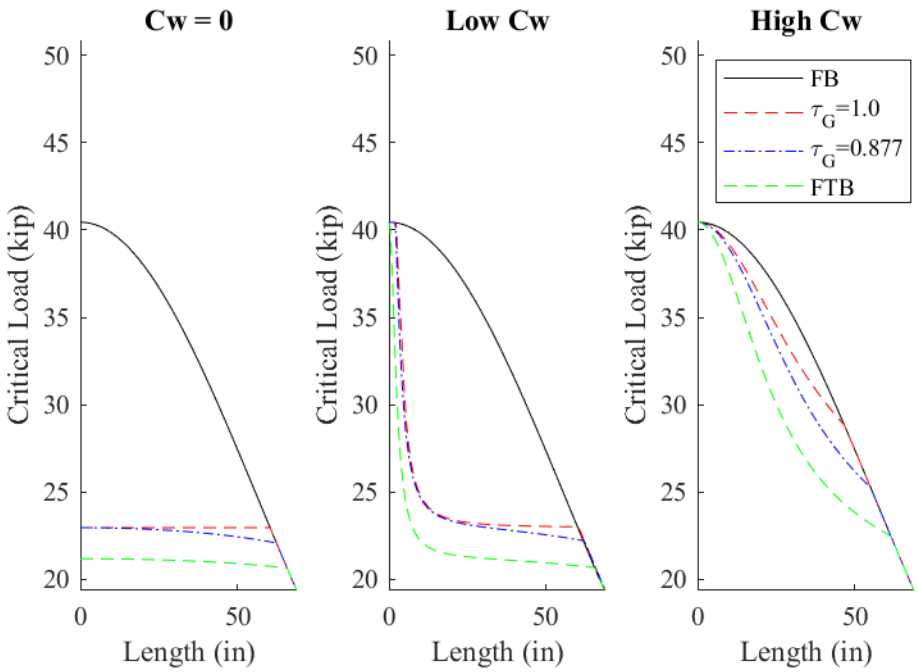

Figure 5: Inelastic buckling of a 2-L2"x2"x0.125" with significant flexural-torsional buckling

inch (22 mm) solid rod diagonal. The joists were both laterally supported and loaded along the top chord at the panel points.

Advanced finite element models of the full joist models were developed in Abaqus (Dassault Systems, 2015) including multiple material models, connection methods, and imperfections. All structural angles were modeled using S4R shell elements while the rod sections were represented by C3D8R solid elements. The joist was evaluated using 4 different material models shown in Fig. 6. All models considered E = 29,000 ksi (200 GPa) and F_y = 50 ksi (345 MPa). The base material model was an elastic-plastic relationship following Eurocode 3 with a post yield modulus of elasticity equal to $E/10000$ (EN 1993-1-5, 2009). Another Eurocode 3 material model was implemented considering linear strain-hardening that began immediately after yield with a stiffness of $E/100$ until ultimate stress was reached at 65 ksi (448 MPa). The third material model was a trilinear approach accounting for an initial perfect plasticity after yield. Strain-hardening started at 10 times the yield strain and was approximated by a linear transition to an ultimate strain of 0.15 in/in and ultimate stress of 65 ksi (448 MPa), which is an effective stiffness of E/267. The fourth and final material model was a realistic reference stress-strain curve for A992-50 taken from literature (ASM International, 2002).

The flare bevel weld connecting the solid rod web to the double angle chord was modeled using a surface to surface tie over the approximate welded area as depicted in Fig. 7. The web connections required consideration of the crimped geometry of the web members as shown in Fig. 8 and modeling of the fillet weld, Fig. 9. The fillet weld was modeled as either: (1) the entire face of the welded region was treated as bonded to the chord (the red area) or (2) only the edge along the physical fillet weld was connected (the blue line). Additionally, each connection alternative

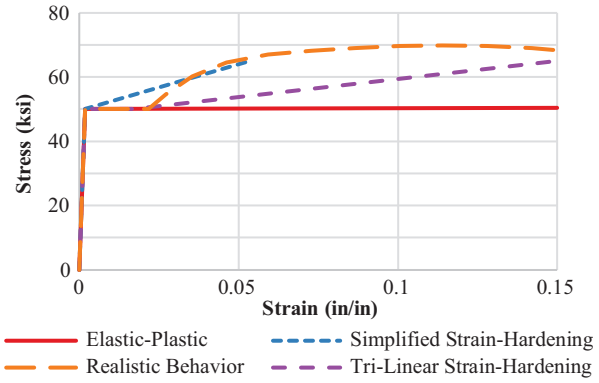

Figure 6: Material models for joist modeling

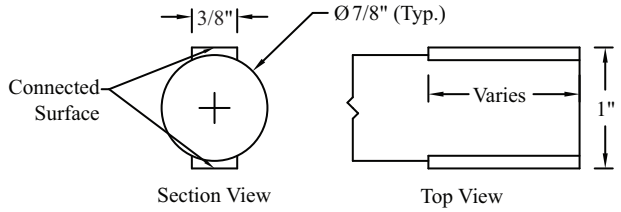

Figure 7: Typical solid rod to angle connection model

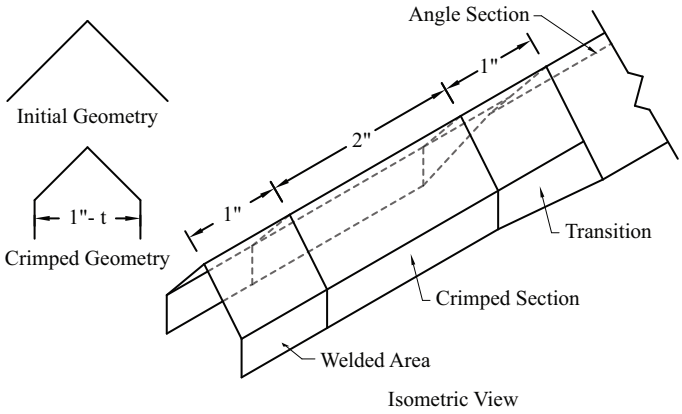

Figure 8: Crimped web geometry

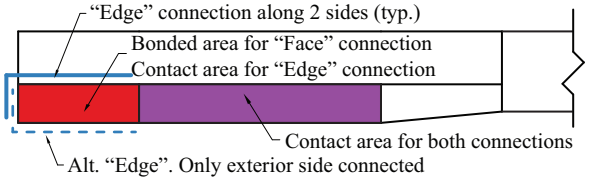

Figure 9: Crimped web end weld model

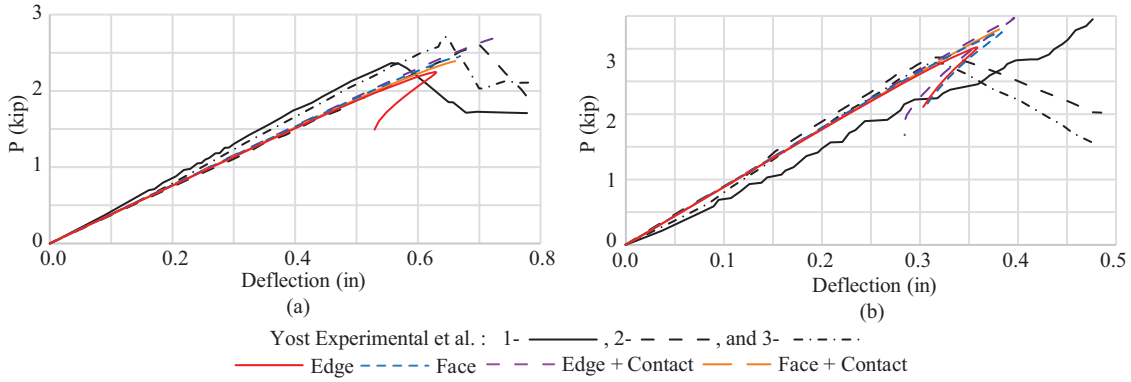

Figure 10: Load-displacements results of validation modeling. (a) 18 in. joist (b) 30 in. joist

Table 2: Ultimate load variation due to connection and material models

Maximum Applied Load, P, (kip)									
Joist Size		18 in. Deep				30 in. Deep			
	Yost et al. (2006)	2.35	2.61	2.70		2.81	2.88	3.35	
	Connection Model	Edge	Face	Edge + C	Face + C	Edge	Face	Edge + C	Face + C
Mat. Model	Elastic-Plastic	2.25	2.44	2.39	2.69	3.02	3.25	3.30	3.47
	Simplified Str.-Hard.	2.20	2.46	2.41	2.68	3.03	3.27	3.30	3.47
	Tri-Linear Str.-Hard.	2.32	2.50	2.46	2.72	3.05	3.36	3.33	3.46
	Realistic	2.28	2.48	2.42	2.68	3.03	3.29	3.30	3.47

was modeled as excluding or including contact between the members resulting in four connection models (the purple area plus the red area for edge connection).

Imperfections were applied to the joist in a half wavelength, sinusoidal distribution along the undeformed length of webs and to the chords between the panel points. Various combinations of in-plane translation, out-of-plane translation, and a rotation were considered in the validation process incorporating translations of $L/1000$, $L/750$, and $L/250$ and rotations of $1/100^{\circ}$ and $1/50^{\circ}$ with a limited selection discussed in this paper. Elastic eigenbuckling imperfections were not implemented as the eigenbuckling results provided irrelevant displacements due to the unsupported bottom chord.

The failure loads and load-deflection information from Yost et al. (2004; 2006) was used to validate the choice of material and connection model for the joist. When including a $L/1000$ out-of-plane imperfection, all combinations of material and connection models captured a similar joist stiffness until approaching failure. Only minimal increases in stiffness occurred due to utilizing the face connection or considering contact. With regard to the elastic-plastic material model, the computational results were found to be in agreement with the softest of the 18 inch deep joists and the stiffest of the 30 inch deep joists as shown in Fig. 10(a) and 10(b), respectively.

The ultimate load, summarized in Table 2, and failure mode of the webs determined using the computational results were in agreement with the experimental behavior. The 18 inch deep steel joist failed in a twisting and bulging mode as shown in Fig. 11. The models consistently failed near the web mid-height while the experimental failure was closer to the crimped geometry transition. It is

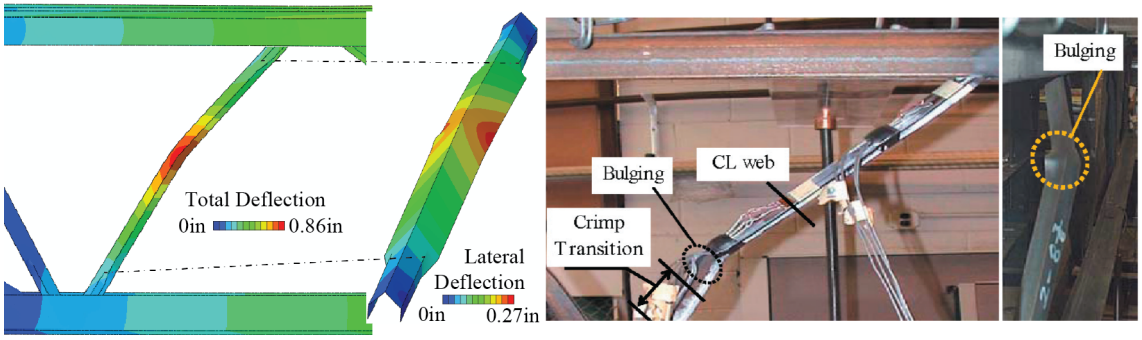

(a) (b)

Figure 11: Twisting and bulging of 18 in. deep joist diagonal at failure. (a) Model (b) Yost et al. (2006)

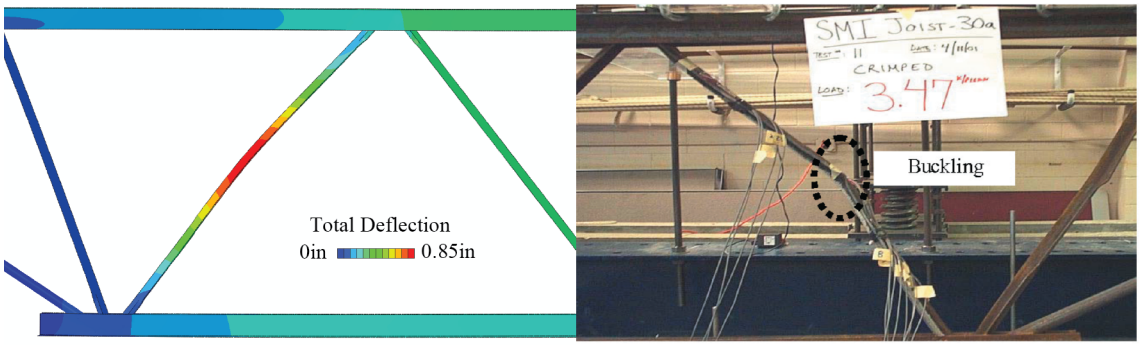

(a) (b)

Figure 12: Flexural buckling of 30 in. deep joist diagonal at failure. (a) Model (b) Yost et al. (2006)

hypothesized that the different failure position is a consequence of the modeling assumptions including (1) the largest imperfections at midspan and (2) not accounting for residual stresses due to the crimping process. The 30 inch deep steel joist was controlled by an in-plane flexural buckling failure mode depicted in Fig. 12. The buckled geometry shown resulted from the edge connection without contact model and the elastic-plastic material relationship. While all connection models resulted in appropriate failure loads, the exclusion of contact captured similar failure modes, provided a more conservative result, and improved run times. It was decided not to use the face connection alternative as it was uncertain how the greater bonded area would correlate to the edge connection alternative. The larger web sizes would provide a sizeable area that would result in a substantially stiffer connection than the edge connection only. Furthermore, the buckled geometry of 30 inch deep joist including contact captured an unexpected in-plane downwards flexural buckling failure, which was unlikely to occur. With respect to the material models, minimal benefits were observed due to strain-hardening, which is neglected in typical steel member design and inelastic modeling provisions per AISC (2016). Therefore, the edge connection without contact and the elastic-plastic material relationship were used for the remainder of the study.

4. Full joist chord study

A 50-foot long, 30 inch deep joist, as shown in Fig. 13 with members in Table 3, was subjected to uniform uplift to investigate buckling of the bottom chord including continuity and connection effects. The webs were sized to not fail in buckling prior to the chords. Table 4 lists the seven

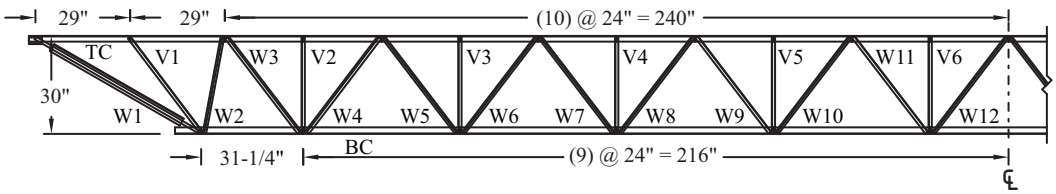

Figure 13: Base geometry of full joist models

Table 3: Joist member cross sections

Label	Member Size
TC	2-L1-3/4”x1-3/4”x0.170”
BC	See Table 4
W1	7/8” Rod + L2-1/2”x2-1/2”x3/16”
W2	CC1-1/4”x1-1/4”x0.188”
W3	CC1-1/2”x1-1/2”x0.25”
W4	CC1-1/2”x1-1/2”x0.138”
W5-W12	CC1-1/4”x1-1/4”x0.125”
V1-V6	L1”x1”x0.109”

different bottom chord double angle cross sections considered in the study. All chord sizes were expected to fail by flexural-torsional buckling at a nominal 4-foot unbraced length.

4.1. Modeling

The joists were modeled as a simply-supported span with the top chord laterally supported on one chord angle at 12 inch o.c. and the bottom chord braced at all panel points. The bottom chord bracing was achieved by incorporating a horizontal bracing angle, which was laterally supported at the ends. A uniformly distributed load was applied over the entire length of the joist top chord via equal point loads on the interior 25% of the cross section as shown in Fig. 14.

Based on the results from the validation study in Section 3., the double angle, single angle, and crimped angle members were modeled with SR4 shell elements and the solid rod webs were modeled using C3D8R solid elements. The web to chord connections utilized the edge connection model without contact to simulate the fillet welds. The double angle chords were connected using vertical segments of 7/8-inch solid rods modeled similar to the end diagonal members as shown in Fig. 15.

The joists were modeled as nominal 50 ksi (345 MPa) yield steel with an elastic-plastic relationship (Fig. 6). Imperfections were applied to the structures in a sinusoidal pattern to each chord with

Table 4: Joist bottom chord cross sections evaluated with advanced modeling

Leg (in)	Thickness (in)			
2	0.125	0.115	0.109	0.094
1.75	0.125	0.115	0.109	

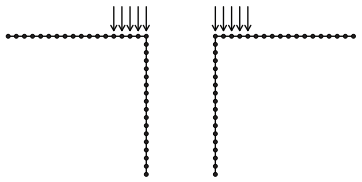

Figure 14: Loading on the top chord cross section

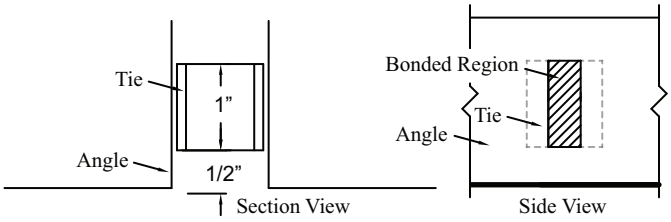

Figure 15: Tie between angle chord details

a half wavelength between the panel points incorporating a $L/1000$ displacement out-of-plane, a $L/1000$ displacement in-plane, and a 1° rotation. Each model was evaluated in a Riks load-controlled analysis to allow for a consistent distribution of load.

4.2. Results

The joist chords exhibited a number of complex displacement patterns at the maximum loading noted in Table 5. The joist chord capacity was consistently observed to be greater than the SJI Specification's flexural buckling limit. The predominant deformation of the chord was in the vertical direction due to the span deflection and twisting of the chord angles as depicted in Fig. 16. The twisting of the chords included a combination of global and local twisting effects that made observations of post-buckling behavior difficult. The complex interaction was confirmed by evaluating the elastic buckling response, which captured five or more buckling modes within 5% of the first mode for each of the 2-in leg angles. Each mode indicated a combination of competing individual angle and composite chord lateral-torsional buckling shapes, all primarily located in the middle three spans. To validate the calculated capacities and to further investigate the complex buckling mode interactions, a chord buckling study was conducted.

Table 5: Full joist modeling results

Member	Model (k)	SJI Design (k)	Model/SJI
2-L2"x2"x0.125"	36.87	30.2	1.22
2-L2"x2"x0.115"	32.09	26.9	1.19
2-L2"x2"x0.109"	28.55	23.4	1.22
2-L2"x2"x0.094"	19.90	19.4	1.03
2-L1.75"x1.75"x0.125"	30.42	25.1	1.21
2-L1.75"x1.75"x0.115"	28.03	22.6	1.24
2-L1.75"x1.75"x0.109"	26.33	20.1	1.31

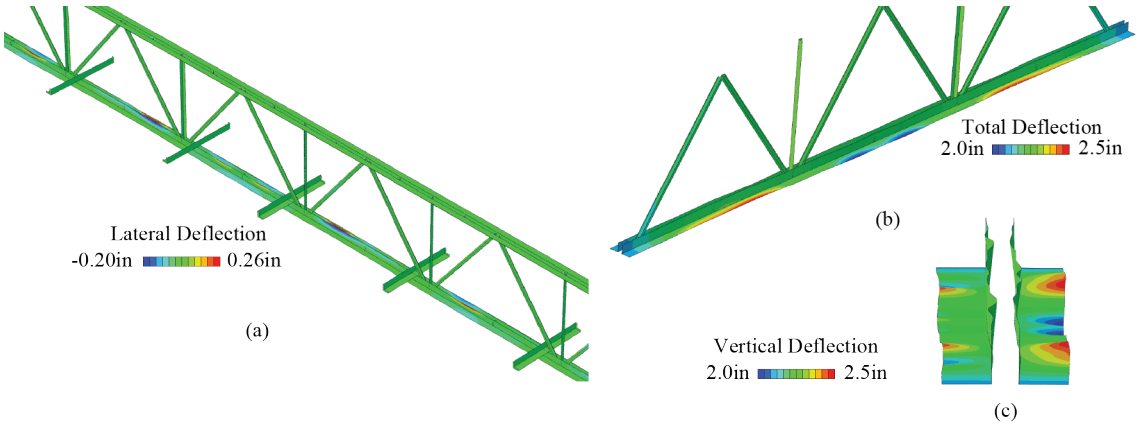

Figure 16: 2-L2"x2"x0.094" joist chord at failure. (a) Lateral displacement of full model. (b) Isometric view of bottom chord. (c) Angled end view of bottom chord.

5. Chord Buckling Study

A simplified double angle chord segment buckling study was completed to validate the full joist modeling results while considering both elastic and inelastic buckling. The seven bottom chord cross sections from Table 4 were evaluated with an effective length, L, of 48 inches with both a pinned-pinned and fixed-fixed boundary condition. This portion of the study varied the number of ties between the chords to account for differences in the composite behavior. While one connection between the double angle chords is typically adequate to meet the minimum requirements of a composite member per the SJI Specification, independent twisting of the individual angles was observed in the full joist investigation. The additional ties were included to capture a more fully composite response.

5.1. Modeling

The double angle chord segment models were based on the same modeling provisions as discussed in Section 4.1. using shell elements for the angles and solid elements for the ties. Each cross section was evaluated with 0, 1, 3, 7, 15, and 23 ties evenly spaced along the length of the chords. The first subset considered a simply supported boundary condition for bending about both the weak and strong axis with a length, L. The pinned boundary condition utilized a rigid tie between a reference node at the centroid and all end nodes on the double angle as shown in Fig 17(a). This node was then subjected to axial load to apply uniform compression to each member. A consequence of this modeling approach was that the end of the members were fixed for warping resulting in a different theoretical effective length in flexural and torsional buckling. As an alternative, a second subset with fixed supports was considered where all end nodes of the member were individually fully restrained as shown in Fig 17(b) to have the same effective length for flexural and torsional buckling. This model was evaluated with a length of $2L$ to keep the same nominal effective length for flexural buckling as the baseline configuration. The fixed support model was loaded by providing a uniform axial displacement across the section. Each model was evaluated for elastic eigenbuckling and then inelastic buckling using the iterative-incremental Riks loading method. The first elastic

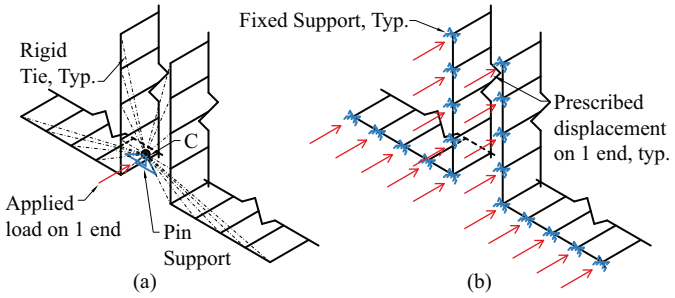

Figure 17: Chord segment end condition. (a) Pinned alternative (b) Fixed alternative

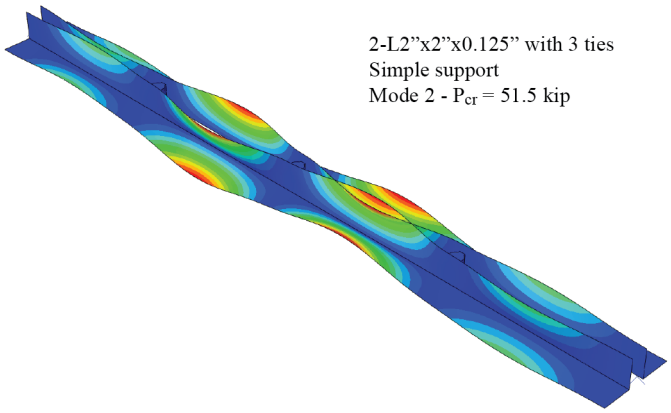

Figure 18: Individual angle flexural-torsional buckling displacement

buckling mode, regardless of the buckled shape, was used as an initial imperfection for the inelastic analyses with a consistent $L/1000$ imperfection for all models.

5.2. Elastic behavior

The elastic buckling investigation depicted a variety of flexural, flexural-torsional, and local buckling responses. Local buckling was observed as either twisting deformations in both flanges of one chord angle, which was classified as individual angles exhibiting flexural-torsional buckling as shown in Fig. 18, or different deformations in the horizontal and vertical flanges resulting in the a non-90° angle between the flanges, which was classified as a distortional buckling mode as depicted in Fig. 19. This change in local buckling was not driven solely by consideration of higher buckling modes, but instead by the amount of tie connectivity between the chords. Considering the results for the 2-L2”x2”x0.125” in Table 6 and 7, distortional buckling behavior was largely limited to configurations with a significant number of connections between the angle members. For most practical joist applications, local buckling of the double angles resulted in single angle flexural-torsional buckling between the ties. Global flexural-torsional buckling was only identified when the ties rotated along with the angles.

It was anticipated that the advanced finite element modeling would capture the same global buckling behavior described in Section 2. with additional local effects. For example, it was estimated

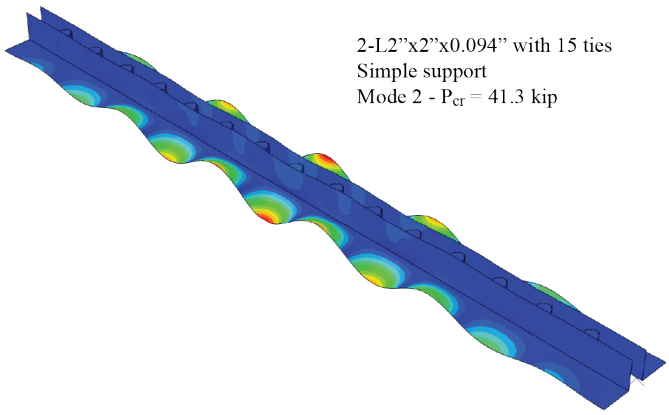

Figure 19: Distortional buckling displacement

Table 6: Elastic buckling of 2-L2"x2"x0.125" chord segment with simple support

Mode		Ties					
		0	1	3	7	15	23
1	P_{cr}	31.7 k	39.5 k	44.4 k	45.9 k	46.3 k	46.5 k
	Shape	g-FB+i-FTB	g-FB+i-FTB	g-FB	g-FB	g-FB	g-FB
2	P_{cr}	40.1 k	43.8 k	51.5 k	71.3 k	95.8 k	98.9 k
	Shape	g-FTB	i-FTB	i-FTB	i-FTB	D	D
3	P_{cr}	42.6 k	44.5 k	51.9 k	71.9 k	95.8 k	99.0 k
	Shape	i-FTB	i-FTB	i-FTB	i-FTB	D	D
4	P_{cr}	42.6 k	44.9 k	52.3 k	72.6 k	97.5 k	100.7 k
	Shape	i-FTB	i-FTB	i-FTB	i-FTB	D	D
5	P_{cr}	44.5 k	46.3 k	52.5 k	73.1 k	97.6 k	100.8 k
	Shape	i-FTB	g-FTB	i-FTB	i-FTB	D	D

FB = Flexural Buckling; FTB = Flexural-Torsional Buckling; D = Distortional
g = Global/composite response; i = Individual angle response

Table 7: Elastic buckling of 2-L2"x2"x0.125" chord segment with fixed support

Mode		Ties					
		0	1	3	7	15	23
1	P_{cr}	18.8 k	32.7 k	39.2 k	44.4 k	45.8 k	46.0 k
	Shape	i-FB	g-FTB	g-FTB	g-FB	g-FB	g-FB
2	P_{cr}	18.8 k	38.6 k	39.3 k	47.5k	65.3 k	84.5 k
	Shape	i-FB	i-FTB	g-FB+i-FTB	g-FTB	g-FTB	g-FTB
3	P_{cr}	33.4 k	38.8 k	43.1 k	51.1 k	70.6 k	89.7 k
	Shape	i-FTB	g-FB+i-FTB	g-FTB	i-FTB	i-FTB	g-FB
4	P_{cr}	33.4 k	39.8 k	43.3 k	51.3 k	70.8 k	90.7 k
	Shape	i-FTB	g-FTB	i-FTB	i-FTB	i-FTB	D
5	P_{cr}	38.1 k	39.8 k	43.7 k	51.5 k	71.1 k	90.8 k
	Shape	i-FB	i-FTB	g-FTB	i-FTB	i-FTB	D

FB = Flexural Buckling; FTB = Flexural-Torsional Buckling; D = Distortional
g = Global/composite response; i = Individual angle response

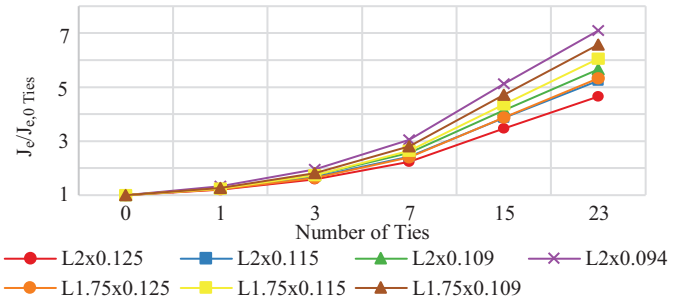

Figure 20: Influence of composite behavior on J_e of double angles

that the 2-L2"x2"x0.125" chord would be controlled by flexural-torsional buckling at approximately 26 kips, which was less than the plate buckling limit. The advanced modeling depicted similar flexural-torsional behaviors with ties spaced at $L/2$, but at a higher load. Additional ties caused the strength to further increase for all buckling modes, but at different rates. Flexural buckling exhibited initial gains due to composite behavior, but an excessive number of ties produced a negligible increase in strength. The torsional behavior of the chord continued to rapidly increase resulting in individual chord angle local buckling to be replaced with a local-distortional response and global flexural-torsional buckling to be significantly greater than the flexural limit. This increase in flexural-torsional buckling was attributed to an increase in torsional stiffness which was confirmed by directly evaluating the models in torsion to determine an effective torsional stiffness, J_e, assuming pure torsion. A single tie was observed to increase the base model stiffness by over 20% as shown in Fig. 20.

5.3. Inelastic behavior

The iterative-incremental inelastic buckling analysis depicted the double angle cross sections primarily failing in flexural buckling that was initiated by the local twisting of the individual angle sections. The buckling strength increased with additional ties, which restrained the twist of individual chords up to a limit where distortion of the flange preceded the onset of buckling. To directly compare the results of the simplified chord models with the full joist models, the number of ties in the simplified chord models was limited to practical numbers such as ties spaced at $L/2$ and $L/4$. It was found that the buckling capacity results, presented in Table 8, were in agreement between the two models for both pinned and fixed boundary conditions. The design limits of both flexural and flexural-torsional buckling were found to underestimate the modeled strength. As the section slenderness increased, the conservatism of the flexural buckling prediction was reduced.

It was expected that the increased torsional stiffness would result in an increased ultimate load for all modeling configurations; however, it was still anticipated that flexural-torsional buckling would occur when considering equal effective lengths for all buckling modes. As noted earlier, the pinned chord model has a reduced effective length for flexural-torsional buckling, which was adequate to change the anticipated failure mode to flexural buckling. Considering the similar buckling capacities from all modeling approaches and the clear flexural buckling response of the simplified chord models, it was concluded that all configurations could provide additional torsional restraint. For

Table 8: Buckling Capacity Comparison

Section	Maximum Model Compression (kip)					Design* (kip)	
	Ties at $L/2$			Ties at $L/4$		FB	FTB
	Joist	Pinned	Fixed	Pinned	Fixed		
2-L2"x2"x0.125"	36.7	34.4	36.7	36.4	35.6	28.3	24.1
2-L2"x2"x0.115"	32.1	31	30.8	33.3	30.7	25.2	20.4
2-L2"x2"x0.109"	28.5	25.7	27.3	25.3	26.6	23.3	18.3
2-L2"x2"x0.094"	19.9	18.5	19.2	18.3	21.5	18.4	13.4
2-L1.75"x1.75"x0.125"	30.2	25	25.5	26.3	26.1	22.8	23.0
2-L1.75"x1.75"x0.115"	28.0	22.8	23.3	24.3	24.1	20.6	19.5
2-L1.75"x1.75"x0.109"	26.3	21.5	22.0	23	22.9	19.3	17.5

* Effective length factors taken as k=1 for all calculations

the joist models and fixed chord models, the continuity of the chord and connection stiffness was theorized to provide additional warping restraint that would normally be conservatively ignored in design.

6. Discussion

The flexural-torsional buckling provisions within the current AISC Specification appear to not take full advantage of known available strength. The conservative approach of utilizing the same elastic-inelastic relationship for flexural and torsional behavior, however, is straight forward. Nevertheless, the capacity of multiple double angle cross sections was observed to be significantly underestimated, as shown in Fig. 3. This reduction is compounded with the recommendation to ignore the C_w of double angles. Without detailed recommendations for determining torsional stiffness for composite members, treating double angles with a warping stiffness and shear center position similar to tee sections appears reasonable for a conservative design. However, this ignores a significant contribution of stiffness, especially when the two angles can act as a composite member. The consideration of both parameters, increased shear stiffness and composite behavior, reduces the likelihood of flexural-torsional buckling controlling the member capacity.

The increased torsional stiffness of the double angles considered in this study resulted in flexural buckling controlling the design behavior. However, that does not mean torsional behavior is not an important component of the limit state. All modeled cross sections were noncompact or slender, which requires the incorporation of local buckling reductions. This local buckling would equate to the flexural-torsional buckling mode of each angle as an independent member (Rasmussen, 2003; Behzadi-Sofiani et al., 2021). For single angles, the flexural-torsional buckling condition does not need to be checked as the local buckling criteria adequately reduces the flexural buckling capacity to address torsional concerns (Galambos, 1991; Rasmussen, 2003), and hence avoids penalizing the capacity of the member twice for the same effect. For double angles, standard engineering practice currently accounts for minimal torsional stiffness benefits, but applies the full penalty of non-compact sections. As a result, designs according to the SJI Specification are only reduced due to local buckling while designs according to the AISC Specification are reduced due to both global and local buckling. Determining an appropriate balance of these factors will be critical to establishing a uniform design approach for all double angle configurations.

7. Conclusions

This paper summarizes a study on flexural-torsional buckling in double angle cross sections for joist and joist girder chords. An inelastic buckling investigation found that while flexural-torsional buckling is not as critical as treated by current AISC design procedures, flexural-torsional buckling is theoretically important for a number of double angle cross sections due to limited nominal torsional stiffness. A series of double angles were evaluated using full joist finite element models that were expected to fail in flexural-torsional buckling. The resulting analysis found that these chords were buckling at or above the SJI flexural buckling limits. The chord deformations were observed to have a combination of local behaviors interacting with the global buckling modes.

An isolated chord segment buckling study was completed to validate the joist study results. Elastic buckling evaluations indicated that local angle behavior between ties was a significant factor in defining the overall deformation of the cross sections. The resulting capacities were greater than the expected theoretical design-based results, while depicting both global and individual angle flexural-torsional buckling. This behavior was due to increased composite torsional stiffness confirmed by additional modeling, but often ignored in design. The increased torsional stiffness caused the inelastic buckling capacity to be controlled by flexural buckling with local twisting of the individual angles.

The preliminary results of this study indicate that the SJI approach of only considering flexural buckling with local buckling reductions seems to be an appropriate design approach for joist chords. The joist chord configuration results in an increased torsional stiffness section property in addition to increased torsional restraint due to continuity and web members. All these factors cause global flexural-torsional buckling behavior to be less significant than the current AISC Specification design approach. The individual twisting of angles cannot be eliminated, but this behavior is accounted for in the local buckling reductions. Further work is in progress to evaluate additional chord dimensions and joist configurations to verify these behaviors in larger double angle sections.

Acknowledgements

The authors would like to thank the Steel Joist Institute for their financial support of this project. The authors would also like to specifically thank Joe Pote and Joe Voigt of New Millennium Building Systems for their input and assistance related to this project.

References

AISC (2010). *Specification for Structural Steel Buildings ANSI/AISC 360-10*. Chicago, IL: American Institute of Steel Construction, p. 609.

AISC (2016). *Specification for Structural Steel Buildings ANSI/AISC 360-16*. Chicago, IL: American Institute of Steel Construction, p. 676.

ASM International (2002). *Atlas of Stress-Strain Curves*. ASM International.

Behzadi-Sofiani, Behnam, Leroy Gardner, M. Ahmer Wadee, Pedro B. Dinis, and Dinar Camotim (2021). "Behaviour and design of fixed-ended steel equal-leg angle section columns". In: *ce/papers* 4.2-4, pp. 1096–1105. DOI: https://doi.org/10.1002/cepa.1400.

CISC (2002). *Torsional Section Properties of Steel Shapes*. Canadian Institute of Steel Construction, p. 19.

Dassault Systems (2015). *Abaqus/CAE*. Johnston, RI: Dassault Systems: V6.16.

EN 1993-1-5 (2009). *Eurocode 3: Design of Steel Structures - Part 1-5: Plated Structural Elements*. European Committee for Standardisation.

Galambos, Theodore V (1963). "Inelastic lateral buckling of beams". In: *Journal of the Structural Division* 89.5, pp. 217–242.

Galambos, Theodore V. (1991). "Design of axially loaded compressed angles". In: *Proceedings of the 1991 SSRC Annual Stability Conference: "Inelastic Behavior and Design of Frames"*. Chicago, IL: SSRC, pp. 353–367.

Kitipornchai, S and HW Lee (1986). "Inelastic buckling of single-angle, tee and double-angle struts". In: *Journal of Constructional Steel Research* 6.1, pp. 3–20.

Neal, B. G. (1950). "The lateral instability of yielded mild steel beams of rectangular cross-section". In: *Philosophical Transactions of the Royal Society of London. Series A, Mathematical and Physical Sciences* 242.846, pp. 197–242. DOI: 10.1098/rsta.1950.0001.

Rasmussen, Kim J.R. (2003). *Design of Angle Columns with Locally Unstable Legs (No. R830)*. URL: https://hdl.handle.net/2123/23919.

Simpson Gumpertz & Heger (2011). *Parameter Study to Assess Modifications to the SJI Design Equations for Buckling of HSLA-V Steels*. Tech. rep. San Francisco, CA: Simpson Gumpertz & Heger, Inc., p. 708.

SJI (2020). *Standard Specifications: Load Tables and Weight Tables for Steel Joists and Joist Girders SJI 100-2020*. 45th Ed. Florence, SC: Steel Joist Institute, p. 232.

Trahair, Nicholas S and Sritawat Kitipornchai (1972). "Buckling of inelastic I-beams under uniform moment". In: *Journal of the Structural Division* 98.11, pp. 2551–2566.

Trahair, Nicholas S. (1993). *Flexural-Torsional Buckling of Structures*. 1st. London; New York: Spon, p. 360. DOI: 10.1201/9781482271218.

Yost, Joseph Robert, David W. Dinehart, Shawn P. Gross, Joseph J. Pote, and James Deeney (2006). "Buckling Strength of Single-Angle Compression Members in K-Series Joists". In: *AISC Engineering Journal* 2, pp. 141–152.

Yost, Joseph Robert, David W. Dinehart, Shawn P. Gross, Joseph J. Pote, and Brian Gargan (2004). "Strength and Design of Open Web Steel Joists with Crimped-End Web Members". In: *Journal of Structural Engineering* 130.5, pp. 715–724. DOI: 10.1061/(ASCE)0733-9445(2004)130:5(715).